

Dynamic hysteresis across a dissipative multi-mode phase transition

Marvin Röhrle¹, Jens Benary¹, Erik Bernhart¹ and Herwig Ott^{1,*}

¹*Department of Physics and Research Center OPTIMAS, University of Kaiserslautern-Landau,
67663 Kaiserslautern, Germany*

(Dated: December 18, 2023)

Dissipative phase transitions are characteristic features in open quantum systems. Key signatures are the dynamical switching between different states in the vicinity of the phase transition and the appearance of hysteresis. Here, we experimentally study dynamic sweeps across a first order dissipative phase transition in a multi-mode driven-dissipative system. In contrast to previous studies, we perform sweeps of the dissipation strength instead of the driving strength. We extract exponents for the scaling of the hysteresis area in dependence of the sweep time and study the $g^{(2)}(0)$ correlations, which show non-trivial behavior. Due to the multi-mode nature of the system, we can also study the influence of the temperature on the hysteresis area. We compare our results to numerical calculations done for a single mode variant of the system, and find surprisingly good agreement. Furthermore, we identify and discuss the differences between a scan of the dissipation strength and a scan of the driving strength.

INTRODUCTION

Open quantum systems are often a more faithful representation of real world systems as compared to a unitary Hamiltonian description of a closed and isolated system. At first glance, the interaction with the environment, which is a native property of open quantum systems, seems to be a nuisance as it introduces dissipation (exchange of particles and energy) and decoherence. However, at second glance, the possible engineering of the environment allows for the robust preparation of quantum states even in the presence of decoherence [1]. Thereby, the intrinsic attractor dynamics provides the means to create such quantum states irrespective of the initial state. Moreover, open systems exhibit new phenomena without a corresponding counterpart in the unitary quantum regime, for instance dynamical switching between different system configurations. A particularly important class of states in open systems are steady-states, whose density operator does not change in time.

In open quantum systems the local conservation of energy and particles is in general no longer valid, since there is a constant exchange with the environment. As a consequence, well established equilibrium concepts have to be adapted for open quantum systems. Most notably, the notion of phase transitions has to be redefined for open systems [2, 3]. Many open quantum systems under investigation are driven-dissipative systems. There, an additional gain mechanism counteracts the dissipation and the steady-states show interesting transport properties for particles, energy, spin, or information. In fact, most transport phenomena in physics are related to the coupling to corresponding reservoirs and are thus best described as an open system. If the properties of such a steady-state change in a non-analytical way upon a change in the system parameters, this is referred to as a dissipative phase transition [3]. Understanding dissipative phase transitions is therefore key to design and en-

gineer transport processes in micro- and nanoscale quantum devices and to harness the system's non-analytic behavior.

Driven dissipative systems are often encountered in photonics. They exhibit metastable states, which can be used for rapid switching, e.g., in lasers [4] and in optical cavities [5, 6]. From early on, optical bistability [7] was found to be a foundational example for a first order dissipative phase transition. When the system is dynamically swept across a first order dissipative phase transition, it exhibits hysteresis. This has been seen in cold atom systems [8–10], Rydberg atoms [11–13], or exciton polariton condensates [14, 15].

For most studied systems it is only possible to dynamically change the driving strength, since the dissipation strength is given by external constraints, e.g., the mirror losses in a cavity. One of the few ways to dynamical change the dissipation or decoherence of a system is via changing the temperature. While this approach works with every experimental system, it is hard to control and depends heavily on the thermalization time of a particular system and the energy spacing of the modes.

In this work we want to leverage our ability to dynamically change the dissipation strength over time to study a bistable system, when sweeping the dissipation strength across the bistable region. We are interested in the similarities and differences to the standard sweeps of the driving strength. Having a multi-mode system at hand, we also investigate the influence of the temperature on the hysteresis behavior.

PHYSICAL SETUP AND THEORETICAL DESCRIPTION

We realize the driven-dissipative system with an ultracold quantum gas of bosonic ^{87}Rb atoms in a one-dimensional optical lattice. Each lattice site contains

a pancake-shaped quasi 2D BEC of about 800 atoms. All lattice sites are coherently coupled to each other with tunneling coupling J . The radial trap frequency is small compared to the chemical potential of each condensate, which makes each pancake a multimode system with more than 80 transverse harmonic oscillator modes occupied. A focused electron beam is used to remove atoms from a single lattice site. This constitutes the loss process in our system. Thereby, the electron beam ionizes the atoms, which are then detected by a channel electron multiplier. This weak probing scheme allows us to continuously monitor the system while creating a local dissipative process. The loss/dissipation rate γ_{diss} is set by the intensity of the electron beam. Since the beam diameter of the electron beam is 150 nm full width half maximum, it can resolve a single lattice site. To create a homogeneous loss over the whole transverse extent, we scan it periodically over the site with high frequency. Tunneling of atoms from neighboring sites into the lossy site constitutes the drive. The steady-state of the system is then determined by the competition between the losses and the inward flow of atoms. This system exhibits a first order dissipative phase transition, which we have analyzed in a precursor study [16]. In Fig. 1 we present a sketch of the experiment.

The studied system can be described theoretically with a multi-mode extension of the seminal Kerr model [7] (all equations with $\hbar = 1$)

$$\hat{H}_{\text{MM}} = \sum_i n_i \omega \hat{a}_i^\dagger \hat{a}_i + \sum_{ijkl} \frac{U_{ijkl}}{2} \hat{a}_i^\dagger \hat{a}_j^\dagger \hat{a}_k \hat{a}_l \quad (1)$$

$$+ \sum_i \left(J_i^* \hat{a}_i e^{i\mu t} + J_i \hat{a}_i^\dagger e^{-i\mu t} \right). \quad (2)$$

The first term describes the occupation of the transverse harmonic oscillator modes in the central site (energy $n_i \omega$), which we chose as a basis for the expansion of the atomic field. The creation and annihilation operators of each mode are denoted by \hat{a}_i^\dagger and \hat{a}_i . The second term is the interaction of the particles in different modes with the interaction matrix elements U_{ijkl} . It allows for a redistribution of the atoms across different modes. The last term is a coherent drive with amplitudes J_i due to tunneling of atoms to and from neighboring sites. The driving frequency is given by the chemical potential μ of the neighboring sites. Note that the tunneling coupling J_i is different for each transverse mode, as the Franck Condon overlap in the tunneling matrix element also depends on the transverse shape of the wave function [16].

The above Hamiltonian is impossible to solve exactly due to the large number of atoms and modes and the all-to-all connectivity of the interaction matrix elements. Recently, there have been two theoretical studies to treat this multi-mode system. One employs a computationally expensive c-field method [17], which can reproduce many

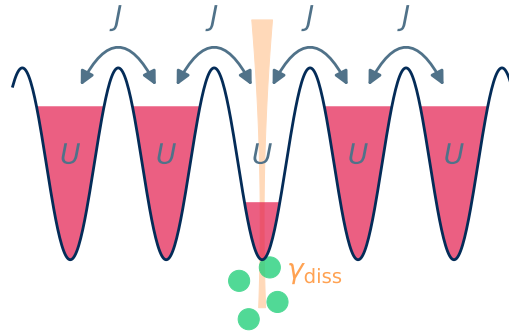


FIG. 1. Sketch of the experimentally studied system. A 1D chain of quasi 2D condensates of rubidium atoms is coupled by the tunneling J . One site is subject to a local loss process, realized by a scanning electron microscope beam, which removes atoms from the cloud and ionizes them. Some of the ions are subsequently detected and are used as a time-resolved measurement signal. Atoms from the neighboring sites can tunnel into the lossy site. More details on the experimental setup can be found in Ref. [16].

of the core results even quantitatively. The other combines the truncated Wigner approximation with a variational ansatz [18], thus being able to reproduce the system dynamics in the absence of dissipation. Dynamical changes of the system parameters, as they are studied in this work, have not yet been addressed theoretically. For the theoretical description in this work, we therefore consider the well-known single mode version of the system's Hamiltonian:

$$\hat{H}_{\text{SM}} = \omega \hat{a}^\dagger \hat{a} + \frac{U}{2} \hat{a}^\dagger \hat{a}^\dagger \hat{a} \hat{a} + F(t)^* \hat{a} e^{i\mu t} + F(t) \hat{a}^\dagger e^{-i\mu t}, \quad (3)$$

where we allow explicitly for a time-dependent external drive $F(t)$. To discern between single mode theory and multi-mode experimental results, the driving strength in the single mode models is written as F , whereas in the multi-mode case as J .

The time evolution is done via a standard master equation in terms of density matrices $\hat{\rho}$ and a Liouvillian superoperator

$$\mathcal{L}\hat{\rho} = \frac{\partial \hat{\rho}}{\partial t} = i \left[\hat{\rho}, \hat{H}_{\text{SM}} \right] + \frac{\gamma(t)}{2} (2\hat{a}\hat{\rho}\hat{a}^\dagger - \hat{a}^\dagger\hat{a}\hat{\rho} - \hat{\rho}\hat{a}^\dagger\hat{a}). \quad (4)$$

The particle losses are described by the dissipation rate $\gamma(t)$, which we also allow to explicitly depend on time. This single mode master equation can be treated numerically for small occupation numbers $\hat{n} = \hat{a}^\dagger \hat{a}$.

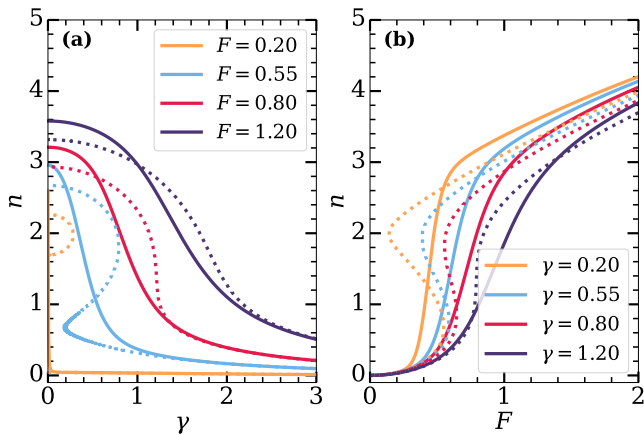


FIG. 2. Steady states of the mean-field model (dotted lines) and master equation (solid lines) when varying γ or F for four different driving strengths F or dissipation strengths γ in (a) and (b), respectively.

Mean-Field Approximation

For the sake of completeness, we also calculate relevant quantities in mean-field approximation. This neglects quantum fluctuations and replaces all operators with complex valued fields. This results in the mean-field equation

$$i\frac{\partial\alpha}{\partial t} = \left(\omega_c - i\frac{\gamma(t)}{2} + U|\alpha|^2\right)\alpha + F(t)e^{-i\omega_p t}, \quad (5)$$

whose time evolution can be computed by numerically integrating the complex valued function α for some initial conditions. The mean particle number in the system is given by $n(t) = |\alpha(t)|^2$. To study hysteresis in the system, either the dissipation strength γ or the driving strength F can be varied over time. Note that functional appearance of the two in Eq. 5 is different. Since the mean-field treatment does no longer explicitly treat quantum effects, it becomes less accurate for small particle numbers. For large occupation numbers instead, it can be a good approximation that agrees with the full quantum treatment of the system [19].

RESULTS

Before we consider the case of dynamically changing a system parameter, let us first theoretically look at the steady states for fixed parameters in order to highlight key differences, when varying the dissipation instead of the driving strength. In Fig. 2 we compare the steady-state for both cases calculated with the master equation and the mean-field approximation. Since the mean-field equation Eq. 5 can not be analytically solved with respect to α when varying γ , the implicit equation is solved nu-

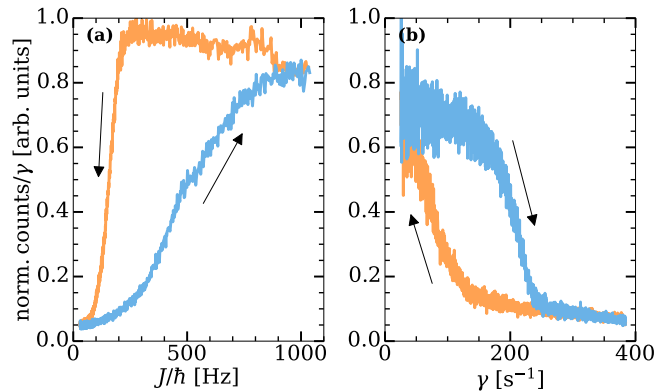


FIG. 3. (a) Hysteresis measurement for a constant dissipation strength $\gamma = 340 \text{ s}^{-1}$ and a linear ramp in the lattice depth, starting with a deep lattice. One direction of the sweep takes $\tau_s = 160 \text{ ms}$ and the hysteresis is averaged over 415 runs. Both parts of the hysteresis are normalized individually. (b) Hysteresis for a constant tunnel coupling $J/\hbar = 290 \text{ Hz}$ and a linear ramp in the dissipation strength γ , starting with a weak dissipation. The sweep time is $\tau_s = 500 \text{ ms}$ and we average over 142 runs.

merically to obtain the steady states. For the master equation, we perform sparse matrix decomposition to obtain the steady state matrix [20]. We then calculate the expectation value for the number operator $\hat{n} = \hat{a}^\dagger \hat{a}$ with the steady state density matrices. Despite the functional difference, how the dissipation and the drive enter the equation of motion (see e.g. Eq. 5) the general behavior is similar. Bistability in the mean-field occurs for certain parameter ranges and the characteristic "S"-shape is recovered in the case of varying the dissipation strength γ as a "Z"-shape. For the master equation, the expectation value is unique in all cases and no signs of bistability occur in either case [7]. However, the steady state $\hat{\rho}_{ss}$ can be a mixture of the mean-field steady states and the system switches between the two [21]. A noticeable difference is that for vanishing dissipation, the mean-field still predicts two stable solutions for small enough drive (Fig. 2(a)). Instead, when keeping the dissipation fixed and changing the drive (Fig. 2(b)), the system always leads to the trivial solution $n = 0$ case for $\gamma > 0$ for small F . Only when $\gamma = 0$, bistability prevails down to $F = 0$. While the basic characteristics are rather similar, one might expect also some differences in the dynamic hysteresis behavior, especially in the limit of small drive and dissipation strength.

Hysteresis measurement

For measuring the hysteresis, we either prepare the system initially with the same occupation number of the central site as compared to the neighboring sites or we remove the atoms from the central site with the elec-

tron beam prior to the experiment, thus starting from an empty site. We then sweep either the dissipation strength $\gamma_{\text{diss}}(t)$ or the tunneling coupling $J(t)$ across the phase transition back and forth for a variable sweep time $2\tau_s$. The time dependent ion signal, which is proportional to the number of atoms occupying the central site, is the basis for the dynamic observation of the system. For each parameter set, we repeat the experiment many times to measure the expectation value and the fluctuations of the atom number.

In Fig. 3, we show the two different types of hysteresis. In both cases, a large hysteresis area is apparent. This confirms that the qualitative behavior for both types of sweeps is the same. Varying the dissipation strength is therefore an equally well suited approach to characterize the hysteresis at a dissipative phase transition as varying the drive strength. In the following, we characterize the hysteresis area and its scaling with the sweep time as well as the fluctuations of the atom number during a hysteresis scan.

Atom number fluctuations

Hysteresis measurements typically concentrate on the evolution of the expectation value of the order parameter of the system. Here, we can also look at the atom number fluctuations across the hysteresis. In Fig. 4 we show the normalized two-body correlation function

$$g^{(2)}(0) = \frac{\langle I^2 \rangle}{\langle I \rangle^2} - \frac{1}{\langle I \rangle}, \quad (6)$$

where I are the ion counts in the central site for a given time bin and $\langle \cdot \rangle$ is the ensemble average over many realizations. In case of no fluctuations beyond Poissonian noise, one would expect a constant value of 1 for the whole protocol. However, we find that within the steep slopes of the hysteresis area, the $g^{(2)}(0)$ value becomes much larger than 1. This indicates large shot to shot fluctuations in the individual realizations of the experiments, corresponding to the system jumping at slightly different times between the two mean-field bistable branches. Note that a value of $g^{(2)}(0) = 2$ corresponds to atom number fluctuations as large as the site occupancy of 800 atoms. The atom number fluctuations are therefore pronounced and a direct consequence of the underlying switching dynamics in the vicinity of the phase transition. Furthermore, in the upper branch of the hysteresis, when the system is in a superfluid state, the $g^{(2)}(0)$ value is around 1. Instead, $g^{(2)}(0)$ is slightly larger than 1 in the lower branch. This reflects the superfluid nature of the steady-state in the upper branch, which suppresses density fluctuations, while the atoms in the lower branch are in a normal state, where bosonic bunching of different modes is present [22]. However, as many modes are

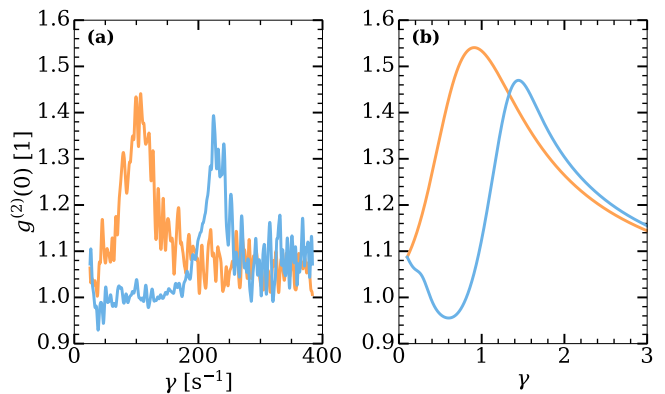


FIG. 4. Normalized pair correlation function $g^{(2)}(0)$ for a hysteresis when sweeping the dissipation. (a) Experimental data corresponding to the hysteresis shown in Fig. 3(b). A Gaussian filter is applied to make the behavior better visible. For further discussion see text. (b) Single mode master equation calculation with driving strength $F = 0.7$ and sweep time $\tau_s = 80$.

involved, the value does not reach $g^{(2)}(0) = 2$ [23]. The corresponding calculation for the single mode system is shown in Fig. 4(b). While the fluctuations also show two maxima, we note that the area in between the maxima shows much larger fluctuations than the experiment. We conclude that the multi-mode nature of the experiment stabilizes the two branches and narrows the parameter range, where the switching occurs.

Scaling of the hysteresis area

Dynamic hysteresis measurements depend on the sweep time, since for an infinitely slow sweep, the system would always be in its steady state and hysteresis would be absent. An important quantity is the hysteresis area A [24], which should vanish for $\tau_s \rightarrow \infty$. The experimentally measured scaling of the area is shown in Fig. 5(a), where an increase for shorter sweep times is clearly visible. The exponent is extracted with a fit to a power law function

$$A \propto \tau_s^\alpha, \quad (7)$$

which directly yields the exponent α . We find an experimental value of $\alpha = -0.87(4)$, when sweeping the dissipation strength.

Theoretically, only the case of sweeping the driving strength $F(t)$ has been studied so far. In mean-field approximation an exponent of $A \propto \tau_s^{-2/3}$ has been found, when sweeping the driving strength F [25]. When doing a similar calculation with a sweep of the dissipation strength $\gamma(t)$ instead, one can find a mean-field exponent of $A \propto \tau_s^{-1}$ [26].

If one includes quantum fluctuations via the master

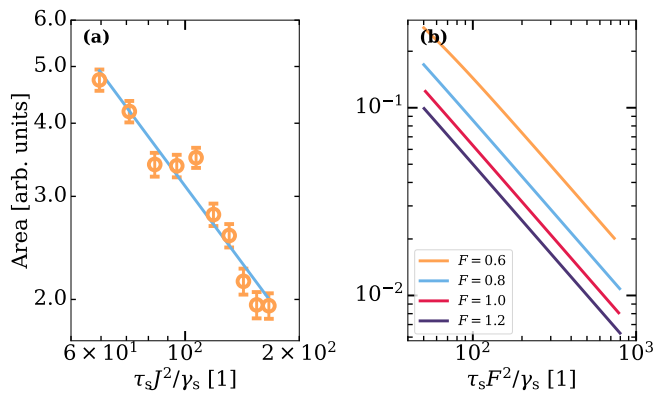


FIG. 5. Scaling of the hysteresis area when sweeping the dissipation strength for different sweep times τ_s . (a) Experimental results for different sweep times. The blue line is a power law fit with an exponent of $\alpha = -0.87(4)$. The hysteresis protocol is the same as in Fig. 3(b). (b) Theoretical results obtained by density matrix time evolution of the master equation. For slow sweeps we find an exponent of $\alpha = -1$, irrespective of the driving strength F .

equation, a sweep of the driving strength in the limit of long sweep times yields a scaling of $A \propto \tau_s^{-1}$ [27]. The same scaling law has been found in other Kerr-type systems, e.g., by a geometric approach [28] or in a Kerr resonator coupled to an ancilla two-level system [29].

To theoretically investigate the influence of quantum fluctuations for our case of a dissipation sweep, we have solved the master equation for the single mode system (Eq. 4). The results are shown in Fig. 5(b). For all studied driving strength values F , we find a scaling exponent of $\alpha = -1$. Thus, in contrast to a sweep of the driving strength, the mean-field and the full quantum description make the same prediction for a sweep of the dissipation strength.

Our experimentally measured exponent of $\alpha = -0.87(4)$ is slightly smaller than the theoretical prediction for the single mode system. At the present stage, it is not clear whether for even longer sweep times, the scaling approaches the value of $\alpha = -1$ or whether the multi-mode system has indeed an intrinsic smaller exponent. A numerical study of the full system can help in this respect, however, up to now, only approximate theoretical models are available (see discussion above).

Temperature dependence of the hysteresis

An intrinsic feature of multi-mode systems is the possibility to exchange population between the modes. This allows for thermalization within the central site and we can address the question, how the temperature of the system affects the hysteresis area. To investigate this regime, we initially prepare a cloud with a higher temperature and corresponding smaller condensate fraction $n_c = N_c/N$.

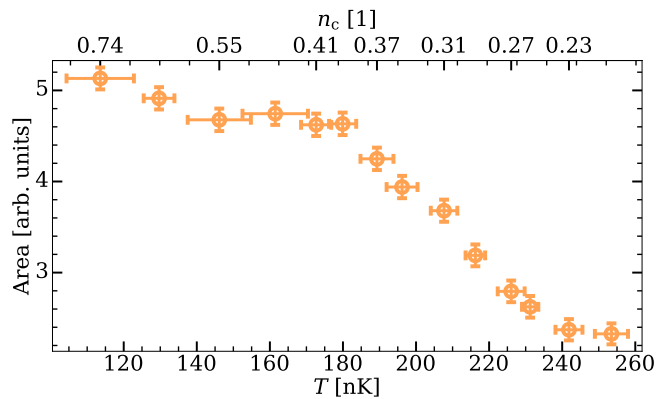


FIG. 6. Hysteresis area at finite temperature. We show the hysteresis area in dependence of the temperature before loading the atoms into the lattice. Note that the number of atoms increases for an initially hotter sample. The hysteresis protocol is the same as in Fig. 3(b). The condensate fraction n_c is given for certain data points individually.

In Fig. 6, we show the hysteresis area for different temperatures when changing the dissipation strength $\gamma(t)$ (J fixed). For higher temperatures the condensate fraction of the sample diminishes and it is clearly visible that the hysteresis area also decreases. Furthermore, the pronounced peaks in the $g^{(2)}(0)$ correlation function vanish for a hotter sample. It is also remarkable that, when decreasing the temperature, the hysteresis area increases faster for higher temperatures, where the condensate fraction increases more strongly, compared to lower temperatures, where most of the atoms are already condensed and the relative condensate growth is less. We conclude that a large condensate fraction, which allows for coherent coupling to the neighboring reservoir sites is important in order for the hysteresis to appear. This can also be understood from the nature of the steady states. In the quantum regime, there are two distinct long-lived steady states, with high and low occupation number. In a thermal system, however, no particular states dominate the system's dynamics and hysteretic behavior is not favored.

Open hysteresis loops

In the discussion of Fig. 2, we have already noticed that in the limit of $\gamma \rightarrow 0$, the mean-field solution does not always become monostable. We now analyze the consequence of this for the hysteresis measurement. To this end, we study the behavior of the hysteresis area for a sweep of the dissipation strength with constant sweep time but varying tunnel coupling J for an initially full site. The results are shown in Fig. 7(a). First, we find that increasing the tunnel coupling between sites increases the hysteresis area. Second, we find that the

hysteresis does not close anymore, if the tunneling coupling is too weak (orange and blue curve in Fig. 7(b)). At first this seems counter-intuitive, however, to understand the reason behind these two phenomena, let us look at each step of the hysteresis and the reaction of the system. When the system is in a state of high occupation number and low dissipation strength, it exhibits coherent perfect absorption [30]. All incoming matter waves are being absorbed and the occupation number stays constant. Increasing the dissipation strength will reach a regime where this effect breaks down. For large driving strengths this break down happens at larger values of the dissipation. Once the system is in the lower branch and the dissipation strength is ramped back again, it does not fully switch back to the high occupation state for small dissipation strengths J (orange and blue curve in Fig. 7(b)) and the hysteresis loop does not completely close. As the refilling behavior is roughly the same for all J , this results in an increase of the hysteresis area with J .

The non-closing of the hysteresis curve is also reproduced by the theoretical model for the single mode system (Fig. 7(c)). However, it shows a decrease in hysteresis area for larger J . This can be viewed as manifestation of macroscopic quantum self-trapping, where the occupation number of the emptied site stays low even for vanishing dissipation strength, due to the difference in chemical potential [31]. In the multimode system at hand, macroscopic self trapping is not possible since the transverse mode splitting is smaller than the chemical potential and resonant tunneling is always possible (at the cost of a reduced Franck Condon overlap, which leads to $J_i < J$ [32]).

SUMMARY AND CONCLUSIONS

To summarize this paper, we have experimentally investigated dynamic hysteresis effects at a first-order dissipative phase transition of a multi mode quantum system by sweeping the dissipation strength γ . We find an asymptotic area scaling exponent slightly smaller than the one predicted by numerical calculations for a full quantum single-mode version of the system. At the edges of the hysteresis area, we find pronounced density-density fluctuations. The hysteresis behavior is less pronounced for increased temperature and - depending on the parameter settings - the hysteresis does not necessarily close.

Our studies extend previous work on hysteresis scaling to many modes and stronger interactions. As the experiments are performed in a regime where exact numerical calculations do not work anymore, they can help to benchmark many-body theories in the vicinity of dissipative phase transitions. For the future, it would be important to develop a better understanding of the universal scaling laws at a dissipative phase transitions - very

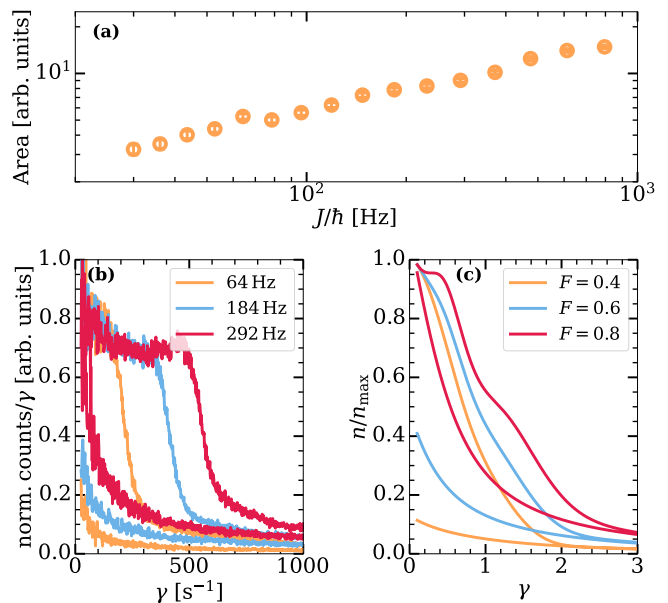


FIG. 7. (a) Hysteresis area in dependence on the tunneling coupling J for sweeps of the dissipation strength. In the hysteresis protocol, we linearly change the dissipation strength γ from 70 Hz to 1800 Hz and $\tau_s = 400$ ms and back, starting from an initially full site. (b) Example of three hysteresis curves for different J/\hbar . They correspond to three data points of (a). The blue and the orange hysteresis loops do not close. (c) Numerical calculations of the single mode system in a similar parameter regime as the experiment. All hysteresis curves are normalized to 1.

much in the same way as it is done with great success for equilibrium phase transitions.

ACKNOWLEDGEMENTS

We would like to thank C. Kollath, M. Fleischhauer, and M. Davis for helpful discussions. The authors acknowledge financial support by the DFG within SFB/TR 185 OSCAR, project number 277625399.

* ott@physik.uni-kl.de

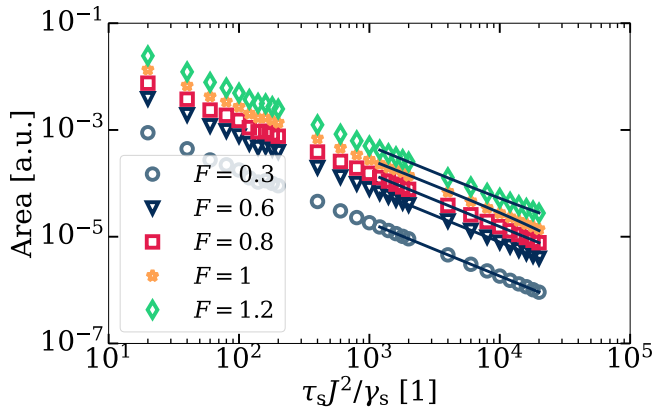
- [1] F. Verstraete, M. M. Wolf, and J. Ignacio Cirac, Quantum computation and quantum-state engineering driven by dissipation, *Nat. Phys.* **5**, 633 (2009).
- [2] E. M. Kessler, G. Giedke, A. Imamoglu, S. F. Yelin, M. D. Lukin, and J. I. Cirac, Dissipative phase transition in a central spin system, *Phys. Rev. A* **86**, 012116 (2012).
- [3] F. Minganti, A. Biella, N. Bartolo, and C. Ciuti, Spectral theory of liouvillians for dissipative phase transitions, *Phys. Rev. A* **98**, 042118 (2018).
- [4] H. Kawaguchi, Bistable laser diodes and their applications: state of the art, *IEEE Journal of Selected Topics in Quantum Electronics* **3**, 1254 (1997).

- [5] G. Rempe, R. J. Thompson, R. J. Brecha, W. D. Lee, and H. J. Kimble, Optical bistability and photon statistics in cavity quantum electrodynamics, *Phys. Rev. Lett.* **67**, 1727 (1991).
- [6] Z. Geng, K. J. H. Peters, A. A. P. Trichet, K. Malmir, R. Kolkowski, J. M. Smith, and S. R. K. Rodriguez, Universal scaling in the dynamic hysteresis, and non-markovian dynamics, of a tunable optical cavity, *Phys. Rev. Lett.* **124**, 153603 (2020).
- [7] P. D. Drummond and D. F. Walls, Quantum theory of optical bistability. i. nonlinear polarisability model, *Journal of Physics A: Mathematical and General* **13**, 725 (1980).
- [8] S. Eckel, J. G. Lee, F. Jendrzejewski, N. Murray, C. W. Clark, C. J. Lobb, W. D. Phillips, M. Edwards, and G. K. Campbell, Hysteresis in a quantized superfluid ‘atomtronic’ circuit, *Nature* **506**, 200 (2014).
- [9] J. Klinder, H. Keßler, M. Wolke, L. Mathey, and A. Hemmerich, Dynamical phase transition in the open dicke model, *Proc. Natl. Acad. Sci. U.S.A.* **112**, 3290 (2015).
- [10] A. Trenkwalder, G. Spagnolli, G. Semeghini, S. Coop, M. Landini, P. Castilho, L. Pezzè, G. Modugno, M. Inguscio, A. Smerzi, and M. Fattori, Quantum phase transitions with parity-symmetry breaking and hysteresis, *Nat. Phys.* **12**, 826 (2016).
- [11] C. Carr, R. Ritter, C. G. Wade, C. S. Adams, and K. J. Weatherill, Nonequilibrium phase transition in a dilute rydberg ensemble, *Phys. Rev. Lett.* **111**, 113901 (2013).
- [12] F. Letscher, O. Thomas, T. Niederprüm, M. Fleischhauer, and H. Ott, Bistability versus metastability in driven dissipative rydberg gases, *Phys. Rev. X* **7**, 021020 (2017).
- [13] D.-S. Ding, H. Busche, B.-S. Shi, G.-C. Guo, and C. S. Adams, Phase diagram and self-organizing dynamics in a thermal ensemble of strongly interacting rydberg atoms, *Phys. Rev. X* **10**, 021023 (2020).
- [14] S. R. K. Rodriguez, W. Casteels, F. Storme, N. Carlon Zambon, I. Sagnes, L. Le Gratiet, E. Galopin, A. Lemaître, A. Amo, C. Ciuti, and J. Bloch, Probing a dissipative phase transition via dynamical optical hysteresis, *Phys. Rev. Lett.* **118**, 247402 (2017).
- [15] L. Pickup, K. Kalinin, A. Askitopoulos, Z. Hatzopoulos, P. G. Savvidis, N. G. Berloff, and P. G. Lagoudakis, Optical bistability under nonresonant excitation in spinor polariton condensates, *Phys. Rev. Lett.* **120**, 225301 (2018).
- [16] J. Benary, C. Baals, E. Bernhart, J. Jiang, M. Röhrle, and H. Ott, Experimental observation of a dissipative phase transition in a multi-mode many-body quantum system, *New Journal of Physics* **24**, 103034 (2022).
- [17] M. T. Reeves and M. J. Davis, Bistability and nonequilibrium condensation in a driven-dissipative josephson array: a c-field model, *arXiv* **2101.02949**, [cond (2021)].
- [18] C. D. Mink, A. Pelster, J. Benary, H. Ott, and M. Fleischhauer, Variational truncated Wigner approximation for weakly interacting Bose fields: Dynamics of coupled condensates, *SciPost Phys.* **12**, 051 (2022).
- [19] N. P. Proukakis and B. Jackson, Finite-temperature models of bose-einstein condensation, *Journal of Physics B: Atomic, Molecular and Optical Physics* **41**, 203002 (2008).
- [20] J. Johansson, P. Nation, and F. Nori, Qutip: An open-source python framework for the dynamics of open quantum systems, *Computer Physics Communications* **183**, 1760 (2012).
- [21] R. M. Wilson, K. W. Mahmud, A. Hu, A. V. Gorshkov, M. Hafezi, and M. Foss-Feig, Collective phases of strongly interacting cavity photons, *Phys. Rev. A* **94**, 033801 (2016).
- [22] V. Guarrera, P. Würtz, A. Ewerbeck, A. Vogler, G. Barontini, and H. Ott, Observation of local temporal correlations in trapped quantum gases, *Phys. Rev. Lett.* **107**, 160403 (2011).
- [23] A. Öttl, S. Ritter, M. Köhl, and T. Esslinger, Correlations and counting statistics of an atom laser, *Phys. Rev. Lett.* **95**, 090404 (2005).
- [24] See Supplemental Material for the definition of the hysteresis area. ().
- [25] P. Jung, G. Gray, R. Roy, and P. Mandel, Scaling law for dynamical hysteresis, *Phys. Rev. Lett.* **65**, 1873 (1990).
- [26] See Supplemental Material for the mean-field calculations of the area scaling law. ().
- [27] W. Casteels, F. Storme, A. Le Boité, and C. Ciuti, Power laws in the dynamic hysteresis of quantum nonlinear photonic resonators, *Phys. Rev. A* **93**, 033824 (2016).
- [28] D. O. Krimer and M. Pletyukhov, Few-mode geometric description of a driven-dissipative phase transition in an open quantum system, *Phys. Rev. Lett.* **123**, 110604 (2019).
- [29] J. Li, H. Z. Shen, W. Wang, and X. Yi, Atom-modulated dynamic optical hysteresis in driven-dissipative systems, *Phys. Rev. A* **104**, 013709 (2021).
- [30] A. Müllers, B. Santra, C. Baals, J. Jiang, J. Benary, R. Labouvie, D. A. Zezyulin, V. V. Konotop, and H. Ott, Coherent perfect absorption of nonlinear matter waves, *Science Advances* **4**, eaat6539 (2018), <https://www.science.org/doi/pdf/10.1126/sciadv.aat6539>.
- [31] S. Raghavan, A. Smerzi, S. Fantoni, and S. R. Shenoy, Coherent oscillations between two weakly coupled bose-einstein condensates: Josephson effects, π oscillations, and macroscopic quantum self-trapping, *Phys. Rev. A* **59**, 620 (1999).
- [32] R. Labouvie, B. Santra, S. Heun, S. Wimberger, and H. Ott, Negative differential conductivity in an interacting quantum gas, *Phys. Rev. Lett.* **115**, 050601 (2015).
]ott@physik.uni-kl.de

Mean-field results

In mean-field approximation, we calculate the scaling laws of the hysteresis area for large sweep times in the following way. We integrate Eq. 5 for some initial condition of α . Unless otherwise stated, we use $\gamma = 1$, $F = \gamma$, $\Delta = -2\gamma$, and $U = \gamma/2$. We start with $\gamma_1 = 5$ and linearly ramp it down to $\gamma_2 = 0.1$ and back up again. This results in a total range of $\gamma_s = |\gamma_1 - \gamma_2| = 4.9$. As initial condition for the population, we use $\alpha = 0$, since for a high dissipation strength the system should have an occupation close to zero. The resulting areas for different driving strengths F are shown in Fig. 1.

For the five different driving strengths shown in Fig. Fig. 1, we find a scaling exponent for large sweep times of -1 . This deviates from the result for a sweep of the driving strength, which was found to scale with an exponent of $-2/3$ [25].



Supplementary Figure 1. Hysteresis area scaling when sweeping the dissipation strength for an initially high dissipation strength for different sweep times τ_s , see text. Five different driving strengths F are shown. The lines correspond to power law fits, each yielding an exponent of -1 .

Hysteresis area calculation

The hysteresis area is defined as

$$A = \left| \int_{t < \tau_s} I(t) dt - \int_{t > \tau_s} I(t) dt \right|. \quad (8)$$

Here, $I(t)$ with $t \in [0, 2\tau_s]$ is the time dependent ion signal which is proportional to the occupation number in the central site.